PCCP

ROYAL SOCIETY OF CHEMISTRY

PAPER

View Article Online
View Journal

Cite this: DOI: 10.1039/d6cp00719h

Resonance enhanced multiphoton ionization studies of di-*ortho*-methoxy methylcinnamate, a cinnamate-based UV-B filter

Ivan Romanov,[a] Michael Hymas,[b] Jack Dalton,[b] Vasilios G. Stavros [b] and Wybren Jan Buma *[ac]

Received 26th February 2026,
Accepted 16th April 2026

DOI: 10.1039/d6cp00719h

rsc.li/pccp

Cinnamate derivatives are considered promising starting points for novel UV filters, using judiciously chosen substitutions on this scaffold to achieve a rational optimization of their properties. Here, we employ electron donating substituents to induce changes in the electronic density distribution of this scaffold and position them such that steric interactions are modulated. Applying high-resolution laser spectroscopic techniques on supersonically cooled compounds in combination with quantum chemical calculations has enabled us to obtain a fundamental understanding of how the electronic structure of ground and electronically excited states as well as their dynamics are affected by such substitutions.

1 Introduction

Cinnamic acids and cinnamates are chromophores employed ubiquitously in natural and artificial UV-filters.[1,2] Their appeal lies in their large extinction coefficients at solar UV radiation wavelengths ($\sim$20 000–30 000 M^{-1} cm^{-1}) and their ability to convert this radiation efficiently into harmless thermal energy, thereby protecting biological tissues from photodamage. However, this energy conversion competes with potentially detrimental pathways such as the formation of long-lived electronically excited states and reactive oxygen species[3,4] which are undesirable and should be minimized. Similar considerations hold for other photothermal applications such as protecting crops against sudden temperature drops during daylight.[5,6]

The spectroscopic properties and excited-state dynamics of cinnamic acid based chromophores are determined by three lower-lying excited singlet states, the V and V′ ππ* states and an nπ* state. The V(ππ*) state is associated with the HOMO → LUMO excitation and has a large oscillator strength, while the V′(ππ*) state with a smaller oscillator strength is described by the (HOMO−1) → LUMO and/or HOMO → (LUMO+1) excitations. The relative order of these states sensitively governs the pathways along which the absorbed photon energy is converted. For unsubstituted cinnamates and coumarates, for example, internal conversion to the nπ* state – which adiabatically becomes the lowest excited singlet state – opens up an efficient intersystem crossing pathway to the triplet manifold[7–10] while for ferulates and sinapates this pathway is significantly less efficient.[11–14] Efforts that rationally modify the electronically excited-state manifold of the cinnamic acid scaffold, and thereby tailor its photochemical and photophysical properties, are therefore widely pursued.[5,15,16]

One of such efforts focussed on exploring how single substitutions with a hydroxy or methoxy group at different positions on the phenyl ring affected these properties.[9,17] In these studies it was concluded that upon *para* substitution both internal conversion to the ground state along *trans* → *cis* isomerisation coordinates as well as the previously mentioned internal conversion to the nπ* state play an important role, while radiative decays dominate the excited-state dynamics of the *ortho* and *meta* substituted compounds. Electron-donating *ortho*-substitutions increase the electronic density on the C_7═C_8 bond (see Fig. 1). One thus expects that energy barriers in the excited state leading to conical intersections with the

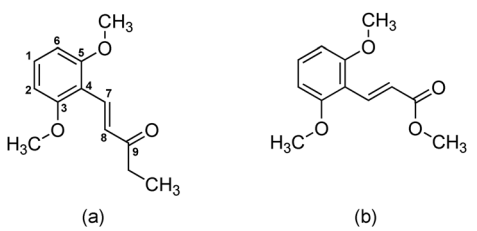

Fig. 1 Molecular structure and atom numbering of di-*ortho*-methoxy methylcinnamate (**1**) with (a) and (b) depicting the s-*cis* and s-*trans* conformers, respectively.

[a] *University of Amsterdam, Van't Hoff Institute for Molecular Sciences, Science Park 904, 1098 XH Amsterdam, The Netherlands. E-mail: w.j.buma@uva.nl*
[b] *School of Chemistry, University of Birmingham, Edgbaston B15 2TT, UK*
[c] *Radboud University, Institute for Molecules and Materials, FELIX Laboratory, Toernooiveld 7c, 6525 ED Nijmegen, The Netherlands*

electronic ground state are lowered by such substitutions, thereby accelerating photon-to-heat conversion and bypassing alternative non-innocent decay pathways. Along a similar reasoning, increasing steric interactions between the phenyl ring and the but-2-enoate part of these compounds is expected to lead as well to a faster geometry relaxation driven by twisting of the $C_7{=}C_8$ bond.

In view of these considerations, it is of great interest to study how substitutions at both *ortho* positions affect the photochemistry and photophysics of the cinnamate scaffold. In the present study we therefore investigate the spectroscopy and dynamics of di-*ortho*-methoxy methylcinnamate seeded in molecular beams. High-resolution laser spectroscopic techniques enable us to record vibrationally-resolved $S_1 \leftarrow S_0$ excitation spectra. Combined with quantum chemical calculations and photoelectron spectroscopy these allow us to conclusively determine the electronic character of the absorbing state, while pump–probe studies elucidate the excited-state dynamics of this state.

2 Methods

2.1 Experimental

The spectrometer and methods have previously been described in detail.[13,14] In the following we will therefore only provide a brief summary and indicate the modifications relevant to the present studies. Di-*ortho*-methoxy methylcinnamate (**1**) was synthesized according to the procedure described previously.[18] A stainless steel oven containing a glass container with **1** was heated to ~140 °C to achieve sufficient vapor pressure. A cold molecular beam was then generated by mixing this vapor with neon gas at a backing pressure of 2 bar, and expanding it into a vacuum using a pulsed valve. After passing a 2 mm skimmer the beam entered a velocity-map imaging (VMI) chamber equipped with a three-plate electrostatic lens allowing for either kinetic-energy-resolved electron detection using electron velocity map imaging (VMI), or time-of-flight based mass-resolved ion detection.

Excitation spectra have been recorded with either one-color (1+1) REMPI using a Nd:YAG pumped dye laser operating on DCM, or two-color (1+1′) REMPI using the aforementioned dye laser system for excitation and an ArF excimer laser (193 nm) for ionisation. Time-resolved decay curves have been obtained by varying the delay between excitation and ionization laser pulses. For UV–UV depletion studies two Nd:YAG pumped dye lasers operating on DCM have been employed. In all cases laser beams were linearly polarised parallel to the detector plane.

2.2 Theoretical

As will be shown below, UV–UV depletion experiments demonstrate that under the employed experimental conditions two conformers of **1** associated with the relative orientation of the $C_7{=}C_8$ and $C_9{=}O$ bonds (see Fig. 1 for structure and atom numbering) and labeled as s-*cis* and s-*trans* can be observed. For each conformer the geometries of S_0, D_0, and T_1 were optimized with (unrestricted) density functional ((U)DFT) at the ωB97XD/cc-pVDZ level,[19,20] as well as the PBE0/cc-pVDZ level[21] in order to enable a direct comparison with calculations previously reported for *ortho*-methoxy methylcinnamate.[17] For the electronically excited states of the neutral and cation, time-dependent DFT (TD-DFT) was employed to optimize their geometries and calculate harmonic force fields. Adiabatic ionization energies were obtained from the energies of the various electronic states at their equilibrium geometry, while vertical ionization energies were determined from (TD)-UDFT calculations on the ionic states at the equilibrium geometries of the electronic state of interest of the neutral molecule. $S_1 \leftarrow S_0$ Franck–Condon spectra have been calculated using the Freq = FC option in Gaussian16, that is, Herzberg–Teller coupling has not been taken into account. All calculations have been performed using the Gaussian16, Rev. C.02 suite of programs.[22]

3 Results and discussion

3.1 Resonance enhanced two-photon ionization excitation spectroscopy

Fig. 2 displays in (a) and (b) respectively one-color (1+1) and two-color (1+1′) resonance enhanced two-photon ionization (R2PI) excitation spectra of **1**. Both spectra show a well-defined first transition at 31 432.6 cm^{-1} – that we will show later to be associated with the $S_1 \leftarrow S_0$ 0-0 transition of the s-*cis* conformer – followed by bands at higher excitation energies of which the transition at 31 532.5 cm^{-1} will be concluded to be associated with the $S_1 \leftarrow S_0$ 0-0 transition of the s-*trans* conformer. These excitation energies imply that the addition of a second *ortho*-methoxy group raises the excitation energy of S_1 by about 700 cm^{-1},[17] bearing in mind that *ortho*-substitution of the bare methylcinnamate scaffold lowers the excitation energy of the $^1\pi\pi^*$ state by ~2600–3000 cm^{-1}.[10] †

Before discussing the excitation spectrum in more detail, two observations merit further attention. The first one is that although the two spectra show resonances at the same excitation energies, it is surprising to find that the intensity distribution over these bands is completely different. The explanation for these large differences is provided by photoelectron spectroscopy studies that will be discussed below. These show that with one-color excitation a two-photon level is reached that is barely above the adiabatic ionization energy of the ground state of the cation D_0. As a result, efficient vertical ionization from S_1 is inhibited, leading to a reduced ionization cross section. At higher excitation energies, however, vibrational levels at higher energies in D_0 become accessible leading to more favourable ionization cross sections. In the following we will therefore take the (1+1′) R2PI excitation spectrum as the starting point for further discussions on transition intensities and Franck–Condon factors.

Secondly, below 31 432.6 cm^{-1} a number of low-intensity bands indicated with an asterisk are observed (Fig. S1). It should be noticed that these bands are detected while monitoring the

† In methylcinnamate the $^1n\pi^*$ state is adiabatically S_1 and S_2 is a $^1\pi\pi^*$ state.

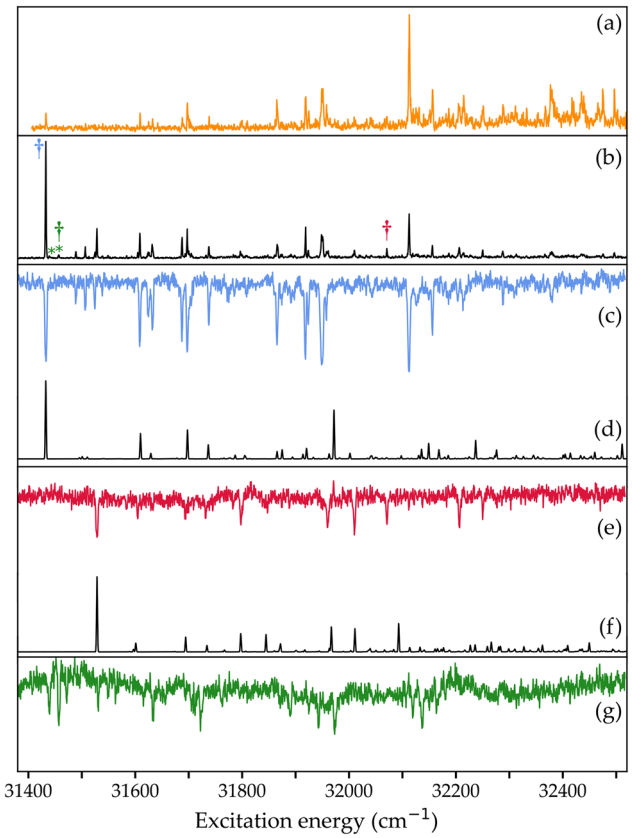

Fig. 2 Jet-cooled excitation spectra of di-*ortho*-methoxy methylcinnamate (**1**) recorded by (a) one-colour (1+1) and (b) two-colour (1+1′) R2PI spectroscopy. Bands indicated with an * in (b) and Fig. S1 are assigned to resonances of **1**-H_2O clusters. (c), (e) and (g) UV–UV depletion spectra obtained at the resonances at 31 432.6, 32 070.9, and 31 457.0 cm^{-1} labelled in (b) with a †. (d) and (f) $S_1 \leftarrow S_0$ Franck–Condon spectra for the s-*cis* and s-*trans* conformers obtained at the PBE0/cc-pVDZ level with 0-0 transitions taken at experimentally observed excitation energies.

mass of the molecular ion. These bands could in principle be associated with another conformer of **1**. However, quantum chemical calculations (*vide infra*) strongly suggest that only the s-*cis* and s-*trans* conformers are expected to be present under our experimental conditions. We have found in our experiments on cinnamates and related compounds that even without explicit introduction of water vapour, water complexes are commonly detected.[7,12,13,23–25] We therefore attribute these bands to transitions associated with excitation of the S_1 state of **1**-H_2O complexes. From the observation that these transitions are detected at the mass of the molecular ion of **1** and that at the mass of **1**-H_2O no signals are observed, we conclude that these complexes dissociate upon excitation and/or ionization. The lowest-energy of these bands is observed at 30 802.3 cm^{-1} implying a red shift of 630.3 cm^{-1}. Such a shift is somewhat larger than observed for *para*-methoxy methylcinnamate (∼130–200 cm^{-1}),[17] in closer agreement with the shifts observed for *para*-hydroxy methyl cinnamate (∼650–700 cm^{-1}),[23,26,27] methyl ferulate (∼530 cm^{-1})[13] and methyl sinapate (∼820 cm^{-1}).[12]

In Fig. 2(c) and (e) UV–UV depletion spectra obtained at 31 432.6 and 32 070.9 cm^{-1} are shown. Apart from a few bands with very low intensity, these two spectra feature all the bands that are observed in the R2PI excitation spectrum of Fig. 2(b). We therefore conclude that under the employed experimental conditions two conformers of **1** are present. In agreement with such a conclusion, quantum chemical calculations (*vide infra*) find that **1** has two low-energy conformations – the s-*cis* and s-*trans* conformations (see Fig. 1) – with the latter predicted to be ∼340 cm^{-1} higher in energy. Based on this energy difference we thus assign the spectra in (c) and (e) to the s-*cis* and s-*trans* conformations, respectively. Monitoring the transition at 30 802.3 cm^{-1} – which was assigned to a conformer of the **1**-H_2O complex – gives rise to the depletion spectrum shown in Fig. 2(g). This spectrum nicely accounts for virtually all the remaining weak features in the excitation spectrum of (b) that had not been covered in (c) and (e). Conversely, it also indicates that assignment of the weaker features in the R2PI excitation spectrum of (b) should be undertaken with caution.

In molecular beam experiments on *ortho*-methoxy methylcinnamate two conformers were detected as well.[17] An explicit assignment of these conformers was not given, but in view of the present results it is most likely that the low-intensity A-labelled conformer is associated with the s-*trans* conformer, and the dominant B-labelled conformer with the s-*cis* conformer. It is interesting to notice (i) that for *ortho*-methoxy methylcinnamate the s-*trans* conformer is the one with the lowest 0-0 excitation energy – as opposed to **1** for which the reverse holds –, and (ii) that the energy difference between the 0-0 transitions of the two conformers is much smaller (8 *vs.* 100 cm^{-1}).

Inspection of the (1+1′) R2PI excitation spectrum and associated depletion spectra leads to the conclusion that the excitation spectra of both the s-*cis* and s-*trans* conformers are dominated by a strong 0-0 transition and show limited vibrational activity. As such it thus appears that excitation of **1** is not accompanied by significant structural changes. Previous studies on substituted cinnamates[11–13,28] have shown that commonly active modes are the in-plane C_4–C_7=C_8 bending mode *b* and the C_7–C_8=C_9 (O) scissor (S) modes, which are found here for the s-*cis* (s-*trans*) conformer at 73.8 (76.3) and 175.4 (166.0) cm^{-1}, as well as the the out-of-plane butterfly β and C_4–C_7 torsion/symmetric methoxy torsion τ of which the overtones are found here at 56.4 and 92.2 cm^{-1} for the s-*cis* conformer. In the present case we find that practically all lower-frequency bands can be assigned in terms of in-plane normal modes and of the previously mentioned overtones or combinations of the out-of-plane β and τ modes. This strongly suggests that the molecule remains planar upon excitation as non-planarity would be accompanied by activity of the fundamental and Franck–Condon progressions of the out-of-plane mode(s) along which the molecule would be distorted.

In previous molecular beam studies on phenyl-substituted cinnamates such as coumarates,[23,26,29] ferulates,[13] and sinapates[11,12] it has been observed that excitation spectra normally display a Franck–Condon progression of the bending mode *b* with an specific activity that depends on whether the V(ππ*) or V′(ππ*) state is excited, but also on the particular conformer that is studied. For **1** the activity of this bending mode is quite limited; only a low-intensity band is observed for the b_0^1

transition and no further activity of overtones can be discerned. We attribute tentatively this lack of activity in part to the increase in steric interactions between the two *ortho* methoxy groups and the hydrogen atoms on C_7 and C_8. Interestingly, while the activity of the bending mode *b* is limited, other low-frequency in-plane modes show a higher activity than observed for other substituted cinnamates indicating that along these modes larger structural changes occur upon excitation than in these previously studied cinnamates.

3.2 Quantum chemical calculations

Quantum chemical calculations performed at the ωB97XD/cc-pVDZ and PBE0/cc-pVDZ levels both find that **1** has two low-energy conformers with an energy difference of $\sim$340 cm^{-1}. In the first instance one might have expected that these conformers would not be planar because of steric interactions, but instead the molecule is found to retain planarity. TD-DFT calculations at these two levels, on the other hand, lead to different results, primarily due to the fact that the V($\pi\pi^*$) and V′($\pi\pi^*$) states are nearly degenerate. The substitution of a second *ortho*-methoxy substituent thus clearly has a significant effect on the excitation energies of the lower electronically excited singlet states as in the study of *ortho*-methoxy cinnamate[17] at the PBE0/cc-pVDZ level it was found that the two $\pi\pi^*$ states were both vertically as well as adiabatically separated by $\sim$0.6 eV.

Table 1 – in which the vertical and adiabatic excitation energies of the lower electronically excited states of the s-*cis* conformer of **1** are reported – shows that calculations at the ωB97XD/cc-pVDZ level find that for vertical excitation S_1 is the V($\pi\pi^*$) state, while S_2 and S_3 are associated with the V′($\pi\pi^*$) and nπ^* states, respectively. At the PBE0/cc-pVDZ level, however, the order of the two $\pi\pi^*$ states is reversed, that is, S_1 is the V′($\pi\pi^*$) state while S_2 is predicted to be the V($\pi\pi^*$) state. Similar observations are made for the s-*trans* conformer for which calculated energies are reported in Table 2.

Geometry optimization of the S_1 (V($\pi\pi^*$)) state at the ωB97XD/cc-pVDZ level under C_s symmetry restrictions leads to s-*cis* and s-*trans* structures at which the difference in S_0–S_1 transition energies is 29 meV (see Tables 1 and 2), which is in good agreement with the observed energy difference between the 0-0 transitions of the two conformers (12 meV). However, calculation of the harmonic force fields shows for both conformers an out-of-plane mode with an imaginary frequency, indicating that these structures do not correspond to the equilibrium geometry of the molecule in S_1. In fact, non-planar S_1 geometry optimization of s-*cis* is found to lead to a true minimum that is 266 cm^{-1} lower in energy and characterized by a C_4–C_7=C_8–C_9 dihedral angle of 164°. A similar optimization for s-*trans*, on the other hand, does not result in a stable minimum but leads to a conical intersection with S_0.

The results obtained at the ωB97XD/cc-pVDZ level do not mirror the experimental trends. First of all, we notice that the calculated S_1 adiabatic excitation energy is more than 0.3 eV higher than the experimentally observed one, and this is higher than what commonly is observed at this level of theory. Likewise, and perhaps more notable is the fact that Franck–Condon simulations of the $S_1 \leftarrow S_0$ excitation spectrum predict extensive progressions of the C_4–C_7 torsional mode. One could argue that the potential energy surface of S_1 is in reality a double-minimum potential with a barrier of only 266 cm^{-1} separating the two minima, and that tunneling would lead to an effective planar structure. However, in such a case extensive activity of this mode would still be expected, which is not observed experimentally.

Calculations at the PBE0/cc-pVDZ level provide in contrast results that are in excellent agreement with the experiment. Geometry optimization of S_1 (in this case the V′($\pi\pi^*$) state) leads to a planar geometry with adiabatic zero-point corrected excitation energies of the s-*cis* and s-*trans* conformers of 3.863

Table 1 Vertical and adiabatic electronic excitation energies (eV) of the lower-lying electronically excited singlet states of s-*cis* **1** under C_s symmetry restrictions with oscillator strength given in parentheses. Calculations at ωB97XD/cc-pVDZ and PBE0/cc-pVDZ levels

	ωB97XD/cc-pVDZ		PBE0/cc-pVDZ	
	Vertical s-*cis*	Adiabatic s-*cis*	Vertical s-*cis*	Adiabatic s-*cis*
V($\pi\pi^*$)	4.500 (0.58)	4.211 (0.66)	4.299 (0.56)	[a]
V′($\pi\pi^*$)	4.596 (0.10)	[b]	4.180 (0.12)	3.975 (0.08)
^{1}nπ^*	4.952 (2×10^{-4})	4.327 (0.0000)	4.529 (1×10^{-4})	3.864 (0.0000)

[a] Geometry optimization leads to root switching with V′($\pi\pi^*$) state. [b] Geometry optimization leads to root switching with V($\pi\pi^*$) state.

Table 2 Vertical and adiabatic electronic excitation energies (eV) of the lower-lying electronically excited singlet states of s-*trans* **2** under C_s symmetry restrictions with oscillator strength given in parentheses. Calculations at ωB97XD/cc-pVDZ and PBE0/cc-pVDZ levels

	ωB97XD/cc-pVDZ		PBE0/cc-pVDZ	
Transition	Vertical s-*trans*	Adiabatic s-*trans*	Vertical s-*trans*	Adiabatic s-*trans*
V($\pi\pi^*$)	4.534 (0.59)	4.240 (0.66)	4.315 (0.58)	[a]
V′($\pi\pi^*$)	4.603 (0.08)	[b]	4.197 (0.08)	3.983 (0.06)
^{1}nπ^*	4.933 (2×10^{-4})	4.409 (1×10^{-4})	4.464 (2×10^{-4})	3.871 (0.0000)

[a] Geometry optimization leads to root switching with V′($\pi\pi^*$) state. [b] Geometry optimization leads to root switching with V($\pi\pi^*$) state.

and 3.873 eV, which almost exactly reproduce the experimental values of 3.897 and 3.910 eV. Similarly, the Franck–Condon spectra predicted for the $S_1 \leftarrow S_0$ transition shown in Fig. 2(d) and (f) nicely match the experimentally observed excitation spectra of these two conformers. We thus conclude (i) that the state observed in the experiments is the V′(ππ*) state, and (ii) that the ωB97XD/cc-pVDZ level cannot adequately describe the electronic structure of the lower-lying electronically excited states of **1**. The latter conclusion is somewhat surprising as the ωB97XD functional has been extensively (and successfully) used in previous quantum chemical calculations on cinnamates.[9,10,15]

The conclusion that in Fig. 2 the V′(ππ*) state is observed and the prediction that the V′(ππ*) state and V(ππ*) states are nearly degenerate automatically raises the question where absorptions to the V(ππ*) state take place. In the case of methyl coumarate – for which an analogous ordering and proximity of the V′(ππ*) state and V(ππ*) states occurs – a careful comparison of R2PI and LIF excitation spectra combined with a clear difference in band widths of resonances $\sim$700 cm^{-1} above the $S_1 \leftarrow S_0$ 0-0 transition enabled us to identify the onset of S_2 (V(ππ*)) $\leftarrow S_0$ transitions.[29] In the present case, however, the excitation spectrum does not give indications for the presence of bands associated with transitions to the V(ππ*) state. We therefore conclude that these transitions either occur at higher excitation energies than explored here, or that this state has such a short lifetime that it cannot be observed under the presently employed nanosecond excitation conditions. Support for the latter hypothesis is found in recent femtosecond time-resolved ion-yield and photoelectron spectroscopic studies that show biexponential decays with a $\sim$3 ps component attributed to the decay of the V(ππ*) state.[18]

For *para*-substituted hydroxy or methoxy methylcinnamates it has been concluded that the dominant decay pathway of the lowest excited singlet state involves the triplet manifold.[7–9,29] Such a pathway is mediated by internal conversion of the ^{1}ππ* state to a lower-lying ^{1}nπ* state, followed by efficient intersystem crossing to the T_1 (^{3}ππ*) state,[30] and to a minor extent by direct intersystem crossing of the ^{1}ππ* state to the T_2 (^{3}nπ*) state followed by internal conversion in the triplet manifold.[8] As such, the ordering of electronically excited singlet states is important. PBE0 calculations predict that adiabatically the ^{1}nπ* state is lower in energy than the V′(ππ*) state. In the studies on *ortho*-methoxy methylcinnamate.[17] it was concluded that the barrier for accessing the ^{1}nπ* state precludes efficient internal conversion. For **1** the energy difference between the two states is about twice as large. This could lead one to hypothesize that in **1** this barrier is lower since the ^{1}nπ* state will cross the V′(ππ*) state at lower energies. In the following we demonstrate, however, using both pump–probe and photoelectron spectroscopy that triplet-mediated decay channels play at most a minor role.

3.3 Excited-state dynamics

Fig. 3 displays (1+1′) pump–probe traces obtained after excitation at the $S_1 \leftarrow S_0$ 0-0 transitions of the s-*cis* and s-*trans* conformers of **1** at 31 432.6 and 31 532.5 cm^{-1}, respectively.

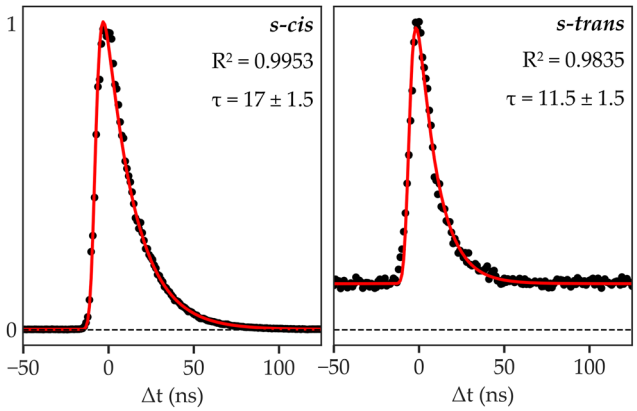

Fig. 3 Time-resolved (1+1′) R2PI decay curves after excitation at the $S_1 \leftarrow S_0$ 0-0 transition of the s-*cis* and s-*trans* conformers of **1**. The solid lines are monoexponential fits convoluted with a Gaussian profile with decay times in nanoseconds.

Analysis of these traces by fitting a Gaussian function with a width of 6 ns to the cross-correlation between the two laser beams, and convoluting it with an exponential decay leads to decay times of 17.0 ± 1.5 and 11.5 ± 1.5 ns for s-*cis* and s-*trans*, respectively. Such decay times are similar to – but slightly longer than – the fluorescence lifetimes measured in LIF studies on *ortho*-methoxy methylcinnamate[17] and in line with the radiative lifetimes as predicted by our PBE0/cc-pVDZ calculations (19.5 and 22.5 ns for s-*cis* and s-*trans*, respectively). It is important to notice that radiative lifetimes calculated from the transition dipole strength of the V(ππ*) $\leftarrow S_0$ transition are an order of magnitude shorter, in clear disagreement with our experimental observations. We thus conclude that the observed excited-state lifetime provides further support for a V′(ππ*) assignment of the state that is excited in our experiments.

In the case of sinapates[12] and ferulates[13] it was concluded that the nπ* state is adiabatically higher in energy than the ππ* state. As a result, intersystem crossing to the triplet manifold is expected to be considerably less efficient as was confirmed by pump–probe studies in which biexponential decays were observed with a dominant few-nanosecond decay involving in part intersystem crossing to the triplet manifold and only a very minor contribution of a longer-lived component associated with the decay of T_1. The monoexponential character observed here is in line with a scenario in which intersystem crossing is 'absent', and the observed decay only due to radiative and nonradiative decay pathways of S_1 to the ground state.

Further insight into the electronic properties of S_1 and the dynamics that occur after excitation of S_1 has been obtained by recording photoelectron (PE) spectra using electron VMI. Fig. 4(a) and 5(a) show to this purpose PE spectra of the s-*cis* and s-*trans* conformers of **1**, respectively, obtained after one-colour (1+1) R2PI. In contrast to *ortho*-methoxy methylcinnamate, for which the ionization potential was concluded to be larger than twice the S_1–S_0 transition energy,[17] we find for **1** that under such conditions the total absorbed energy is slightly larger than the D_0 adiabatic ionization energy. As a result, the

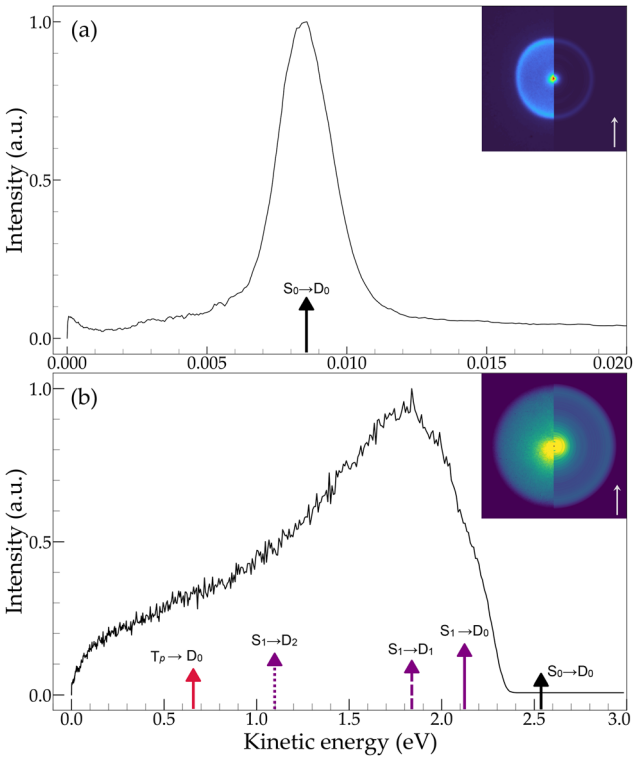

Fig. 4 PE spectra of the s-*cis* conformer of **1** obtained after one- (a) and two-colour (b) R2PI *via* the $S_1 \leftarrow S_0$ 0-0 transition at 31 432.6 cm^{-1}. The inset shows in the left half the recorded image while the right half presents the reconstructed slice through the centre of the original 3D distribution with the arrow indicating the electric field polarisation of the laser pulse(s).

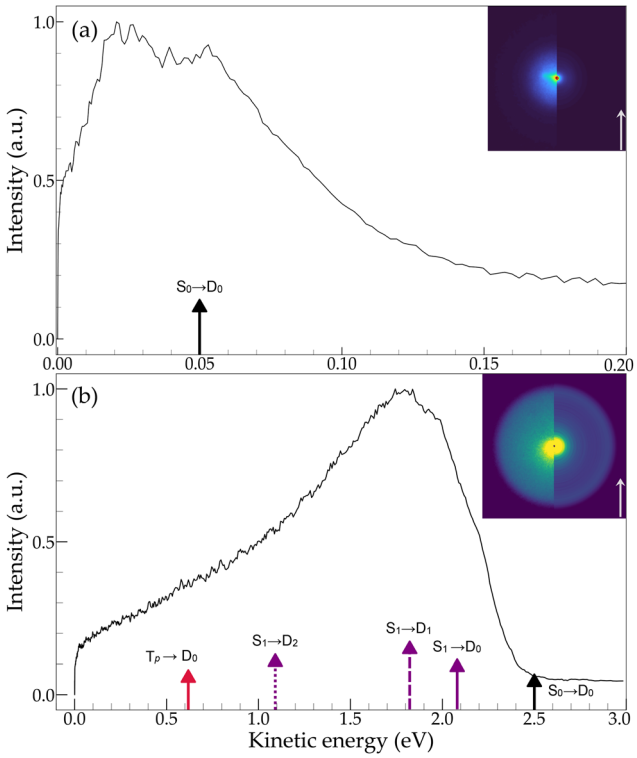

Fig. 5 PE spectra of the s-*trans* conformer of **1** obtained after one- (a) and two-colour (b) R2PI *via* the $S_1 \leftarrow S_0$ transition at 32 070.9 cm^{-1}, chosen as it is the only band in the excitation spectrum of this conformer that is clearly separated from bands of other species (see Fig. 1). The inset shows in the left half the recorded image while the right half presents the reconstructed slice through the centre of the original 3D distribution with the arrow indicating the electric field polarisation of the laser pulse(s).

adiabatic ionization energy associated with ionisation of the vibrationless level of S_0 to the vibrationless level of D_0 – leading to photoelectron kinetic energies indicated by the black solid arrows in Fig. 4(a) and 5(a) – can be determined quite accurately, and is found to be 7.786 ± 0.001 and 7.900 ± 0.005 eV for the s-*cis* and s-*trans* conformer, respectively. Similar to our previous studies on cinnamate-based UV filters[14] we find that these energies are considerably higher ($\sim$0.4 eV) than the energies predicted by our quantum chemical calculations. For the analysis of PE spectra recorded under (1+1′) R2PI conditions discussed below we will therefore use the experimentally determined D_0 adiabatic ionization energy as a starting point, and predict adiabatic and vertical ionization energies to the electronically excited states of the ion using calculated (TD)-UDFT excitation energies of these states.

Panels (b) of Fig. 4 and 5 display (1+1′) R2PI PE spectra obtained at the same excitation energies as in (a) but using 193 nm to ionise the electronically excited state. From an energy point of view several other ionization pathways are in principle available under such conditions. These include ionization to electronically excited states of the ion, but also ionization from the triplet manifold. For the latter pathway we assume that ionization takes place from highly-excited vibrational levels of T_1 that would have become populated after intersystem crossing from the vibrationless level of S_1. Franck–Condon considerations then suggest that these levels will predominantly ionize to vibrational levels in the ion with the same amount of vibrational energy, for which we take the energy difference between the optimized S_1 and T_1 states. In these panels the kinetic energy associated with adiabatic $D_0 \leftarrow S_0$ ionization as determined from the one-colour PE spectrum is indicated with the black solid arrow, while kinetic energies predicted for transitions from electronically excited states are indicated by purple and red arrows for vertical ionization from S_1 and T_1, respectively, with line styles representing transitions to different ionic states (solid lines to D_0, dashed lines to D_1, and dotted lines to D_2). Above we have concluded that calculations at the ωB97XD/cc-pVDZ level do not describe adequately the lower-lying electronically states of **1**. Predictions of photoelectron kinetic energies for various ionisation pathways as indicated in panels (b) are therefore based on our calculations at the PBE0/cc-pVDZ level.

The PE spectra in panels (b) show that ionization from S_1 predominantly occurs to the first electronically excited state of the cation D_1 with a further contribution from ionization to D_0, the ground state of the ion. According to our TD-DFT calculations the $V'(\pi\pi^*)$ state is described by a dominant contribution from the HOMO−1 → LUMO excitation, but also has a contribution from the HOMO → LUMO excitation, while for the $V(\pi\pi^*)$ state the reverse holds (see Table S1). Since D_0 and D_1 are basically described by the $(\text{HOMO})^{-1}$ and $(\text{HOMO}-1)^{-1}$

configurations, propensity rules for ionization[31,32] predict that ionization of the V′(ππ*) state will primarily occur to D_1. Since this is exactly what is observed, the PE spectra thus confirm our conclusion drawn on the basis of the vibrational activity in the $S_1 \leftarrow S_0$ excitation spectrum that S_1 is associated with the V′(ππ*) state.

Our pump–probe spectra led to the conclusion that within our detection limits no evidence is found for a triplet-mediated decay channel. The same is concluded from the PE spectra since these do not show any distinct band in the kinetic energy region where photoelectrons associated with ionization from T_1 are expected. It is interesting to notice that photoelectrons – albeit with a minor intensity – can be detected in the kinetic energy region where ionization to D_2 is predicted. Since this ionic state is primarily described by the $(n)^{-1}$ configuration, such a $D_2 \leftarrow S_1$ pathway could become active if the V(ππ*) state would be vibronically coupled to the ^{1}nπ* state. However, considering the bandwidths that are observed in (1+1′) photoelectron spectra of other cinnamates,[14] it is more likely that the observed activity is part of the Franck–Condon activity associated with the $D_0 \leftarrow S_1$ and $D_1 \leftarrow S_1$ pathways.

4 Conclusions

The cinnamate scaffold is an attractive, naturally occurring starting point for the further development of UV light absorbers that serve either purely for protecting from the harmful effects of UV radiation but may also serve as a means to convert photon energy into other forms of energy such as heat. In the present studies we have focussed on how substitution of this scaffold with electron donating groups at both *ortho* positions of the phenyl ring influences the electronic and spectroscopic properties of the scaffold, and which excited-state decay pathways are available after photon absorption. Excitation spectra obtained with one- and two-color R2PI in combination with UV-depletion spectroscopy show that under the employed molecular beam conditions the molecule can adopt two conformations with very similar properties. Interestingly, comparison of the Franck–Condon activity in these spectra with quantum chemical predictions has led to the conclusion that the observed electronically excited singlet state is the V′(ππ*) state and not the V(ππ*) state. Such a conclusion finds further support in photoelectron spectra recorded upon excitation of this state, which show a dominant ionization pathway to D_1 and a minor contribution from ionization to D_0. As such, the ordering of the ^{1}ππ* states follows what is observed for coumaric acid based derivatives, noticing that for ferulic and sinapic acid based derivatives the reverse ordering is found.

Quantum chemical calculations indicate that adiabatically the ^{1}nπ* state is the lowest excited singlet state. For coumarates this has been found to enable a very efficient intersystem crossing pathway to the triplet manifold. In the present case, however, – and in line with what was found for the mono *ortho*-substituted compound – this pathway is absent. Instead, a monoexponential decay is observed that suggests that radiative decay is the dominant channel with nonradiative $S_1 \rightarrow S_0$ pathways playing only a minor role.

Originally we hypothesized that increasing electron donating effects and combining them with increased steric hindrance might lead to a more facile access to the S_1–S_0 conical intersection. The present experiments have demonstrated that such is not the case when methoxy substituents are used. However, the goal to rationally engineer the potential energy surfaces of electronically excited states of cinnamates using other judiciously chosen substituents in order to improve their performance is still highly promising. We are presently therefore exploring the photophysical and photochemical properties of differently substituted cinnamates using similar methodologies as used in the present work.

Author contributions

I. R. and W. J. B. conceived the study. I. R. performed the spectroscopic experiments and performed the quantum chemical calculations together with W. J. B. J. D., M. H., and V. G. S. contributed to the critical evaluation of the work and provided critical feedback on the manuscript. W. J. B. supervised the work. All authors contributed to writing the manuscript.

Conflicts of interest

There are no conflicts to declare.

Data availability

Supplementary information (SI) is available. See DOI: https://doi.org/10.1039/d6cp00719h.

Data for this article including Fig. 2–5 and Fig. S1 are available at Zenodo at https://doi.org/10.5281/zenodo.18784133.

Acknowledgements

This project has received funding from the European Unions Horizon 2020 research and innovation programme under the grant agreement No. 828753. J. D. and V. G. S. acknowledge funding through EPSRC under the grant agreement No. UKRI2691. We gratefully acknowledge drs. Hans Sanders for the synthesis of **1**.

Notes and references

1 R. Shuab, R. Lone and K. K. Koul, *Acta Physiol. Plant.*, 2016, **38**, 64.
2 B. Rioux, J. Combes, J. M. Woolley, N. D. N. Rodrigues, M. M. Mention, V. G. Stavros and F. Allais, *Front. Chem.*, 2022, **10**, 886367.
3 K. M. Hanson, E. Gratton and C. J. Bardeen, *Free Radical Biol. Med.*, 2006, **41**, 1205–1212.
4 J. Kockler, M. Oelgemöller, S. Robertson and B. D. Glass, *J. Photochem. Photobiol., C*, 2012, **13**, 91–110.

5 T. T. Abiola, B. Rioux, J. M. Toldo, J. Alarcan, J. M. Woolley, M. A. P. Turner, D. J. L. Coxon, M. Telles do Casal, C. Peyrot, M. M. Mention, W. J. Buma, M. N. R. Ashfold, A. Braeuning, M. Barbatti, V. G. Stavros and F. Allais, *Chem. Sci.*, 2021, **12**, 15239–15252.
6 J. M. Woolley, N. D. N. Rodrigues, J. M. Toldo, B. Rioux, C. Groves, X. Schrama, J. Alarcan, T. T. Abiola, M. M. Mention, M. T. do Casal, S. E. Greenough, M. Borja, W. J. Buma, M. N. R. Ashfold, A. Braeuning, T. Munnik, K. A. Franklin, F. Allais, M. Barbatti and V. G. Stavros, *Phys. Chem. Chem. Phys.*, 2025, **27**, 7375–7382.
7 E. M. M. Tan, M. Hilbers and W. J. Buma, *J. Phys. Chem. Lett.*, 2014, **5**, 2464–2468.
8 K. Yamazaki, Y. Miyazaki, Y. Harabuchi, T. Taketsugu, S. Maeda, Y. Inokuchi, S.-N. Kinoshita, M. Sumida, Y. Onitsuka, H. Kohguchi, M. Ehara and T. Ebata, *J. Phys. Chem. Lett.*, 2016, **7**, 4001–4007.
9 S.-n Kinoshita, Y. Miyazaki, M. Sumida, Y. Onitsuka, H. Kohguchi, Y. Inokuchi, N. Akai, T. Shiraogawa, M. Ehara, K. Yamazaki, Y. Harabuchi, S. Maeda, T. Taketsugu and T. Ebata, *Phys. Chem. Chem. Phys.*, 2018, **20**, 17583–17598.
10 S.-n Kinoshita, Y. Inokuchi, Y. Onitsuka, H. Kohguchi, N. Akai, T. Shiraogawa, M. Ehara, K. Yamazaki, Y. Harabuchi, S. Maeda and T. Ebata, *Phys. Chem. Chem. Phys.*, 2019, **21**, 19755–19763.
11 J. C. Dean, R. Kusaka, P. S. Walsh, F. Allais and T. S. Zwier, *J. Am. Chem. Soc.*, 2014, **136**, 14780–14795.
12 J. Fan, W. Roeterdink and W. J. Buma, *Mol. Phys.*, 2021, **119**, e1825850.
13 I. Romanov, Y. Boeije, J. M. Toldo, M. T. Do Casal, M. Barbatti and W. J. Buma, *J. Phys. Chem. A*, 2025, **129**, 36–49.
14 I. Romanov, W. Roeterdink, Y. Boeije, H. Maurer and W. Jan Buma, *Phys. Chem. Chem. Phys.*, 2025, **27**, 17959–17969.
15 S.-n Kinoshita, Y. Harabuchi, Y. Inokuchi, S. Maeda, M. Ehara, K. Yamazaki and T. Ebata, *Phys. Chem. Chem. Phys.*, 2021, **23**, 834–845.
16 T. T. Abiola, N. d N. Rodrigues, C. Ho, D. J. L. Coxon, M. D. Horbury, J. M. Toldo, M. T. do Casal, B. Rioux, C. Peyrot, M. M. Mention, P. Balaguer, M. Barbatti, F. Allais and V. G. Stavros, *J. Phys. Chem. Lett.*, 2021, **12**, 337–344.
17 Y. Miyazaki, K. Yamamoto, J. Aoki, T. Ikeda, Y. Inokuchi, M. Ehara and T. Ebata, *J. Chem. Phys.*, 2014, **141**, 244313.
18 M. Hymas, J. Dalton, I. Romanov, H. Sanders, M. Barbatti, J. M. Toldo, W. J. Buma and V. G. Stavros, *Commun. Chem.*, 2026, DOI: 10.1038/s42004-026-01963-2.
19 J.-D. Chai and M. Head-Gordon, *Phys. Chem. Chem. Phys.*, 2008, **10**, 6615–6620.
20 J. Dunning and H. Thom, *J. Chem. Phys.*, 1989, **90**, 1007–1023.
21 C. Adamo and V. Barone, *J. Chem. Phys.*, 1999, **110**, 6158–6170.
22 M. J. Frisch, G. W. Trucks, H. B. Schlegel, G. E. Scuseria, M. A. Robb, J. R. Cheeseman, G. Scalmani, V. Barone, G. A. Petersson, H. Nakatsuji, X. Li, M. Caricato, A. V. Marenich, J. Bloino, B. G. Janesko, R. Gomperts, B. Mennucci, H. P. Hratchian, J. V. Ortiz, A. F. Izmaylov, J. L. Sonnenberg, D. Williams-Young, F. Ding, F. Lipparini, F. Egidi, J. Goings, B. Peng, A. Petrone, T. Henderson, D. Ranasinghe, V. G. Zakrzewski, J. Gao, N. Rega, G. Zheng, W. Liang, M. Hada, M. Ehara, K. Toyota, R. Fukuda, J. Hasegawa, M. Ishida, T. Nakajima, Y. Honda, O. Kitao, H. Nakai, T. Vreven, K. Throssell, J. A. Montgomery, Jr., J. E. Peralta, F. Ogliaro, M. J. Bearpark, J. J. Heyd, E. N. Brothers, K. N. Kudin, V. N. Staroverov, T. A. Keith, R. Kobayashi, J. Normand, K. Raghavachari, A. P. Rendell, J. C. Burant, S. S. Iyengar, J. Tomasi, M. Cossi, J. M. Millam, M. Klene, C. Adamo, R. Cammi, J. W. Ochterski, R. L. Martin, K. Morokuma, O. Farkas, J. B. Foresman and D. J. Fox, *Gaussian ~ 16 Revision A.03*, Gaussian Inc., Wallingford CT, 2016.
23 M. de Groot, E. V. Gromov, H. Köppel and W. J. Buma, *J. Phys. Chem. B*, 2008, **112**, 4427–4434.
24 J. Fan and W. J. Buma, *J. Phys. Chem. A*, 2023, **127**, 1649–1655.
25 J. Fan and W. J. Buma, *Photochem. Photobiol. Sci.*, 2023, **22**, 2715–2724.
26 S. Smolarek, A. Vdovin, E. M. M. Tan, M. de Groot and W. J. Buma, *Phys. Chem. Chem. Phys.*, 2011, **13**, 4393–4399.
27 E. M. M. Tan, S. Amirjalayer, S. Smolarek, A. Vdovin, A. M. Rijs and W. J. Buma, *J. Phys. Chem. B*, 2013, **117**, 4798–4805.
28 J. Fan, L. Finazzi and W. Jan Buma, *Phys. Chem. Chem. Phys.*, 2022, **24**, 3984–3993.
29 E. M. M. Tan, S. Amirjalayer, B. H. Bakker and W. J. Buma, *Faraday Discuss.*, 2013, **163**, 321–340.
30 M. A. El-Sayed, *Acc. Chem. Res.*, 1968, **1**, 8–16.
31 V. Blanchet, M. Zgierski and A. Stolow, *J. Chem. Phys.*, 2001, **114**, 1194–1205.
32 M. Schmitt, S. Lochbrunner, J. Shaffer, J. Larsen, M. Zgierski and A. Stolow, *J. Chem. Phys.*, 2001, **114**, 1206–1213.

